NUCL SCI TECH (2019) 30:122
https://doi.org/10.1007/s41365-019-0646-7

Effect of Na and Cl ions on water evaporation on graphene oxide

Xi Nan[1,2] · Yu-Wei Guo[1,2] · Rong-Zheng Wan[1]

Received: 27 March 2019 / Revised: 18 April 2019 / Accepted: 23 April 2019 / Published online: 12 July 2019

Abstract Using molecular dynamics simulations, we investigate the influence of Na and Cl ions on the evaporation of nanoscale water on graphene oxide surfaces. As the concentration of NaCl increases from 0 to 1.5 M, the evaporation rate shows a higher decrease on patterned graphene oxide than that on homogeneous graphene oxide. The analysis shows an obvious decrease in the evaporation rate from unoxidized regions, which can be attributed to the increased amount of Na^+ ions near the contact lines. The proximity of Na^+ significantly extends the H-bond lifetime of the outermost water molecules, which reduces the number of water molecules diffusing from the oxidized to unoxidized regions. Moreover, the effect of the ions on water evaporation is less significant when the oxidation degree varies in a certain range. Our findings advance the understanding of the evaporation process in the presence of ions and highlight the potential application of graphene oxide in achieving controllable evaporation of liquids.

This work was supported by the National Natural Science Foundation of China (Nos. U1832170 and 11474299) and Computer Network Information Center of Chinese Academy of Sciences.

Electronic supplementary material The online version of this article (https://doi.org/10.1007/s41365-019-0646-7) contains supplementary material, which is available to authorized users.

✉ Rong-Zheng Wan
wanrongzheng@sinap.ac.cn

[1] Division of Interfacial Water and Key Laboratory of Interfacial Physics and Technology, Shanghai Institute of Applied Physics, Chinese Academy of Sciences, Shanghai 201800, China

[2] University of Chinese Academy of Sciences, Beijing 100049, China

Keywords Evaporation · Ions · Graphene oxide · Molecular dynamics simulation

1 Introduction

The evaporation of nanoscale amounts of water on various surfaces is of great interest in many areas, from nature to industry; for instance, evaporation is responsible for huge water losses through soil salinization [1], inorganic salt transport in plants [2], and carbon dioxide capture to mitigate climate change [3]. In the industrial field, evaporation is also a crucial process in printable electronics fabrication [4], spray cooling [5, 6], gold nanorod (GNR) assembly [7], and protein folding [8, 9].

The evaporation of water can be affected by many factors, e.g., surface characteristics [10, 11], temperature [12, 13], and humidity [14, 15]. Recent studies show that the evaporation of small amounts of water is greatly affected by the solid surface wettability and show different characteristics with respect to the evaporation from bulk water surfaces [16–18]. Our previous work showed that the evaporation of small volumes of water on patterned graphene oxide (GO) surfaces is faster than that on homogeneous graphene oxide surfaces [19]. He et al. [20] found that a chemically patterned surface can enhance evaporation by extending the contact lines. Last year, Guo and Wan [21] discovered that the evaporation rate of nanoscale water on uniformly complete wetting surfaces slowly increases with increasing temperature.

Ionic species, which are ubiquitous in nature [22–32], have also been shown to affect the evaporation properties of bulk water and droplets [33–35]. Many studies showed that the presence of impurities slows down the evaporation

of macroscopic water in atmospheric or industrial conditions [36–39]. However, the specific influence of ionic species on the evaporation of small volumes of water on nanoscale surfaces remains unclear.

Herein, using molecular dynamics (MD) simulations, we investigated the influence of sodium and chlorine ions on the evaporation of nanoscale water on GO surfaces. We find that the evaporation rate shows a higher decrease on patterned GO surfaces than that on homogeneous ones. The total evaporation rate on patterned GO surfaces originates from the corresponding rates of both oxidized and unoxidized regions. The decrease in the evaporation rate on patterned GO can be attributed to the obvious decrease in water evaporation from the unoxidized regions. The analysis shows that the increased amount of Na^+ ions near the contact lines significantly reduces the number of water molecules diffusing from the oxidized to the unoxidized regions. Furthermore, the water evaporation from patterned GO does not change significantly until the C/(OH) ratio reaches 10.7: Ions and water molecules can no longer be excluded from the unoxidized region, and the evaporation rate drops. These findings could be useful for achieving controllable evaporation of liquids on graphene oxide surfaces.

2 Computational methods

We investigated patterned and homogeneous graphene oxide nanosheets with dimensions of 14.7 nm × 12.9 nm (Fig. 1a) and carbon–carbon bond lengths of 0.142 nm. A graphene oxide ceiling of the same size was placed 8.7 nm above the substrate. The homogeneous GO and the oxidized regions of patterned GO were built based on a $C_{32}O_n(OH)_n$ molecular formula (Lerf–Klinowski structural model [40]), which means that n epoxy and n hydroxyl groups were decorated on the graphene plane every 32 carbon atoms, where n = 3, 4, 5, 6, or 8 [41]. The unoxidized regions of patterned GO were solid surfaces without oxidative functional groups (Fig. 1b). The oxidized regions have hydrophilic properties associated with the polar oxygen functional groups [42], while the unoxidized regions remain hydrophobic, reflecting the wetting properties of graphene.

Initially, 2256 TIP3P [43] water molecules were arranged in a box placed 0.5 nm above the homogeneous and patterned GO substrates. The initial size of the box was 13.0 nm × 11.0 nm × 0.5 nm. In order to prevent the water molecules from returning to the surface, an accelerating region was set from 1.85 to 4.35 nm above the lower substrate. An upward force of 1.0 kcal mol^{-1} $Å^{-1}$ [force vector (0, 0, 1)] was applied to the oxygen atom when a water molecule entered the accelerating region.

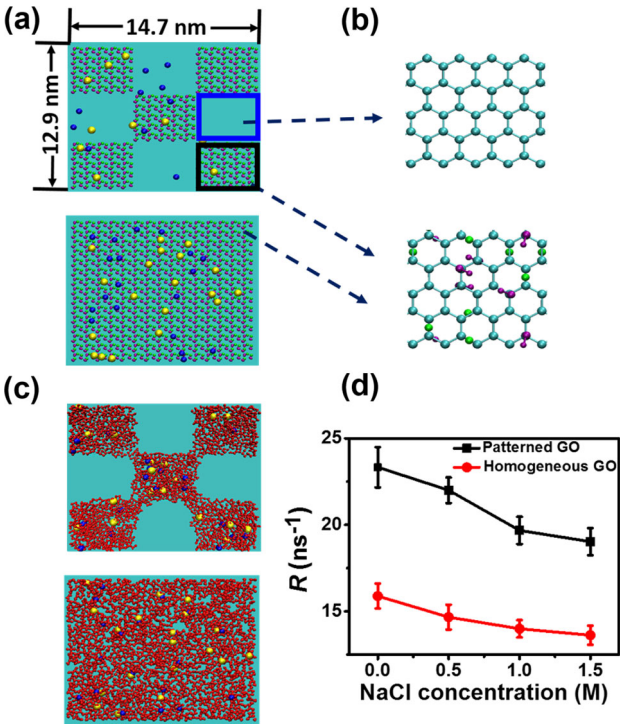

Fig. 1 (Color online) Water evaporation on patterned and homogeneous GO surfaces. **a** Geometry of the patterned and homogeneous surfaces. The blue and black rectangles outline the unoxidized and oxidized regions, respectively. **b** Detailed geometry of the unoxidized and oxidized regions. **c** Snapshot of water and ions on patterned and homogeneous GO surfaces. **d** Evaporation rate on GO surfaces with different NaCl concentrations. The black circles and red squares represent the evaporation rates of patterned and homogeneous GO, respectively

These non-equilibrium settings are equivalent to the conditions applied in other literature studies, in which molecules evaporate into an infinite vacuum [44]. The Na^+ and Cl^- ions were randomly distributed on the surfaces. The ionic concentrations were set to 0.5, 1.0, and 1.5 M, with corresponding total number of ions of 20, 38, and 60, respectively, equally divided between Na^+ and Cl^- ions. Due to the periodic boundary conditions, the evaporated water molecules were absorbed by the solid ceiling and the water molecules under it. The evaporation rate R is defined as the number of water molecules moving from the substrate into the accelerating region per nanosecond.

MD simulations were carried out in a box with initial size of 14.7 nm × 12.9 nm × 11.0 nm, using NAMD 2.10 [45]. The time step of the simulation was 1 fs. Periodic boundary conditions were applied to all Cartesian coordinates. The Lennard-Jones parameters of the carbon atoms were σ = 0.358 nm and ε = 0.0663 kcal mol^{-1}. Charges of 0.2 and 0.266 e were employed for carbon atoms attached to the epoxy and hydroxyl groups, respectively. The Charmm27 force field [46] was used in the simulations. The particle mesh Ewald method [47] was employed to

treat long-range electrostatic interactions, and Langevin dynamics was applied to maintain the system at 300 K. The velocities and coordinates were collected every 500 fs. For all systems, after an equilibrium MD simulation of 2 ns, we applied the accelerating region to five independent systems for 7 ns, and data extracted from the last 5 ns of these simulations were averaged for the subsequent analysis.

3 Results and discussion

Figure 1c shows snapshots of water molecules and ions on both patterned and homogeneous GO surfaces. (The oxidized regions were built based on a $C_{32}O_6(OH)_6$ composition.) The figure shows that both water molecules and ions are distributed only on the oxidized regions. As shown in Fig. 1d, as the concentration of NaCl increases from 0 to 1.5 M, the total evaporation rate decreases for both patterned and homogeneous GO surfaces. In order to understand this decrease, we analyze the averaged total interaction energy E_{Total} of the outermost water molecules, which acts as an energy barrier preventing water molecules from evaporating [48].

In the following, E_{Total} denotes the sum of the water–surface ($E_{\text{Water–surface}}$), water–water ($E_{\text{Water–water}}$), water–Na^+ ($E^{+}_{\text{Water–Na}}$), and water–Cl^- ($E^{-}_{\text{Water–Cl}}$) interaction energies. As shown in Fig. 2a, b, the total interaction energy E_{Total} shows a similar increasing trend on patterned and homogeneous GO. Thus, as the concentration of NaCl increases, the energy barrier associated with the outermost water molecules becomes larger, and the evaporation rate decreases.

For patterned GO surfaces (Fig. 2a), $E^{+}_{\text{Water–Na}}$ and $E^{-}_{\text{Water–Cl}}$ show an obvious increase as the concentration of NaCl increases, whereas $E_{\text{Water–water}}$ and $E_{\text{Water–surface}}$ only exhibit slight changes; these variations result in an overall increase in E_{Total}. A similar trend is observed for homogeneous GO surfaces (Fig. 2b), except for the slight decrease in $E_{\text{Water–surface}}$.

$E_{\text{Water–surface}}$ is mainly affected by the distance between the GO surface and the outermost water molecules (thickness of the water film). Figure 2c shows that, as the

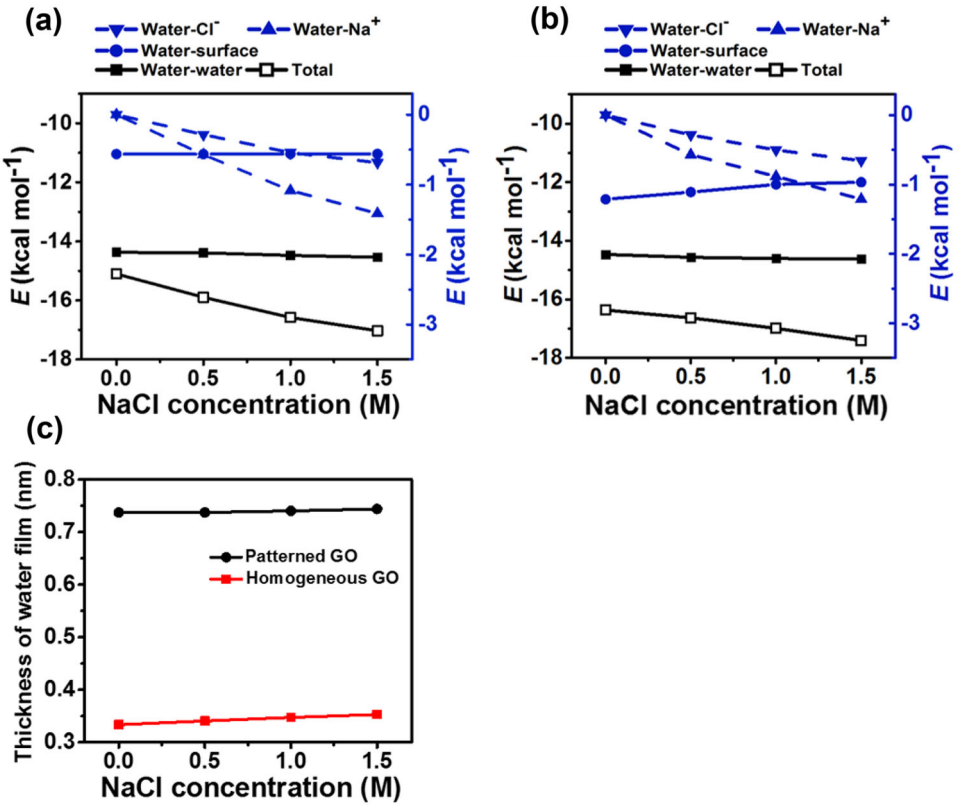

Fig. 2 Changes in average interaction energy per outermost water molecule and water film thickness with NaCl concentration. **a** Average interaction energy per outermost water molecule on patterned GO surfaces. **b** Average interaction energy per outermost water molecule on homogeneous GO surfaces. The blue down-triangles, blue up-triangles, blue circles, and black solid squares represent the average interaction energy between water and Cl^- ($E^{-}_{\text{Water-Cl}}$), water and Na^+ ($E^{+}_{\text{Water–Na}}$), water and GO surface ($E_{\text{Water–surface}}$), and two water molecules ($E_{\text{Water–water}}$), respectively, while the black hollow squares denote the average total interaction energy (E_{Total}). **c** Thickness of water film on patterned and homogeneous GO surfaces with different NaCl concentrations. The black circles and red squares represent the water film thickness on patterned and homogeneous GO, respectively. (Color figure online)

concentration of NaCl increases, the thickness of the water film on the patterned GO surface remains almost constant, because the film is relatively thick. In contrast, the thickness of the relatively thin water film on the homogeneous GO surfaces exhibits an obvious decrease.

It has been reported that water evaporation is enabled by the concerted and ultrafast H-bond dynamics of interfacial water [12]. Thus, we examined the hydrogen bonding characteristics of the outermost water molecules. In particular, two water molecules were considered hydrogen-bonded when their O–O distance and O…O–H bond angle were less than 3.3 Å and 30°, respectively [49]. The average lifetime of the H-bonds, $\tau_{\text{H-bond}}$, was determined by fitting the exponential decay function $y(t) = e^{-t/\tau\text{H-bond}}$. (The result of double exponential fittings of the H-bonds autocorrelation function can be found in the Electronic Supplementary Information, ESI†.) As shown in Fig. 3a, b, as the concentration of NaCl increases, the average number of H-bonds per outermost water molecule shows only a slight decrease on both patterned and homogeneous GO surfaces, while $\tau_{\text{H-bond}}$ shows a significant increase. The presence of the Na^+ and Cl^- ions results in an obvious increase in the $\tau_{\text{H-bond}}$ value for the outermost water molecules and therefore reduces the water evaporation rate.

As shown in Fig. 1d, as the concentration of NaCl increases from 0 to 1.5 M, the total evaporation rate on the patterned GO surfaces decreases by 4.3 ns^{-1} (from 23.3 ± 1.1 to 19.0 ± 0.8 ns^{-1}), while that on the homogeneous GO surfaces only decreases by 2.3 ns^{-1} (from 15.9 ± 0.7 to 13.6 ± 0.6 ns^{-1}). Since the total evaporation rate of patterned GO surfaces derives from the evaporation rates of the oxidized and unoxidized regions [50], we calculated the evaporation rate on both regions with different NaCl concentrations, as shown in Fig. 4. The figure shows that the reduced evaporation from patterned GO surfaces is mainly due to the obvious decrease in evaporation rate from the unoxidized regions.

In order to understand the decrease in evaporation rate on the unoxidized regions, we examined the distribution of ions and water molecules on patterned GO surfaces with different concentrations of NaCl. The results are illustrated in Fig. 5. The reference plane ($z = 0$) for all calculations is the lower one.

Figure 5a–c shows the distribution probabilities of Na^+, Cl^-, and water molecules along the z-direction, for NaCl concentrations of 0.5, 1.0, and 1.5 M. Throughout the concentration range investigated, the figures show that the Na^+ ions are closer to the lower plane than the Cl^- ones. Figure 5d–f shows the Na^+ and Cl^- distribution probabilities and the surface density of water molecules as a function of the distance to the contact line, for NaCl concentrations of 0.5, 1.0, and 1.5 M. Compared with Cl^-, the

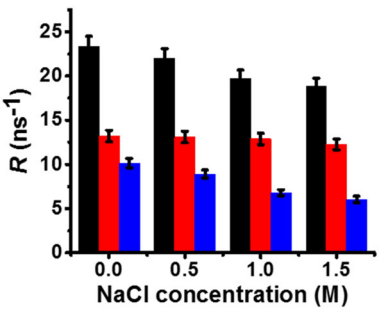

Fig. 4 Evaporation rate on patterned GO surfaces with different NaCl concentrations. The black, red, and blue bars represent the total evaporation rate, the evaporation rate from the oxidized regions, and the evaporation rate from the unoxidized regions, respectively. (Color figure online)

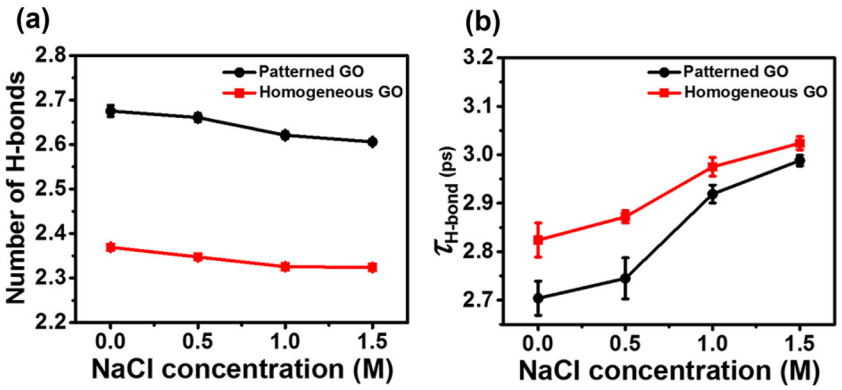

Fig. 3 Hydrogen bonding characteristics of outermost water molecules on patterned and homogeneous GO surfaces with different NaCl concentrations. **a** Average number of H-bonds for outermost water molecules on patterned and homogeneous GO surfaces with different NaCl concentrations. The black circles and red squares represent the average numbers of H-bonds per outermost water molecule on patterned and homogeneous GO surfaces, respectively. **b** Average lifetime of H-bonds for outermost water molecules on patterned and homogeneous GO surfaces with different NaCl concentrations. The black circles and red squares represent the average H-bonds lifetimes for outermost water molecules on patterned and homogeneous GO, respectively. (Color figure online)

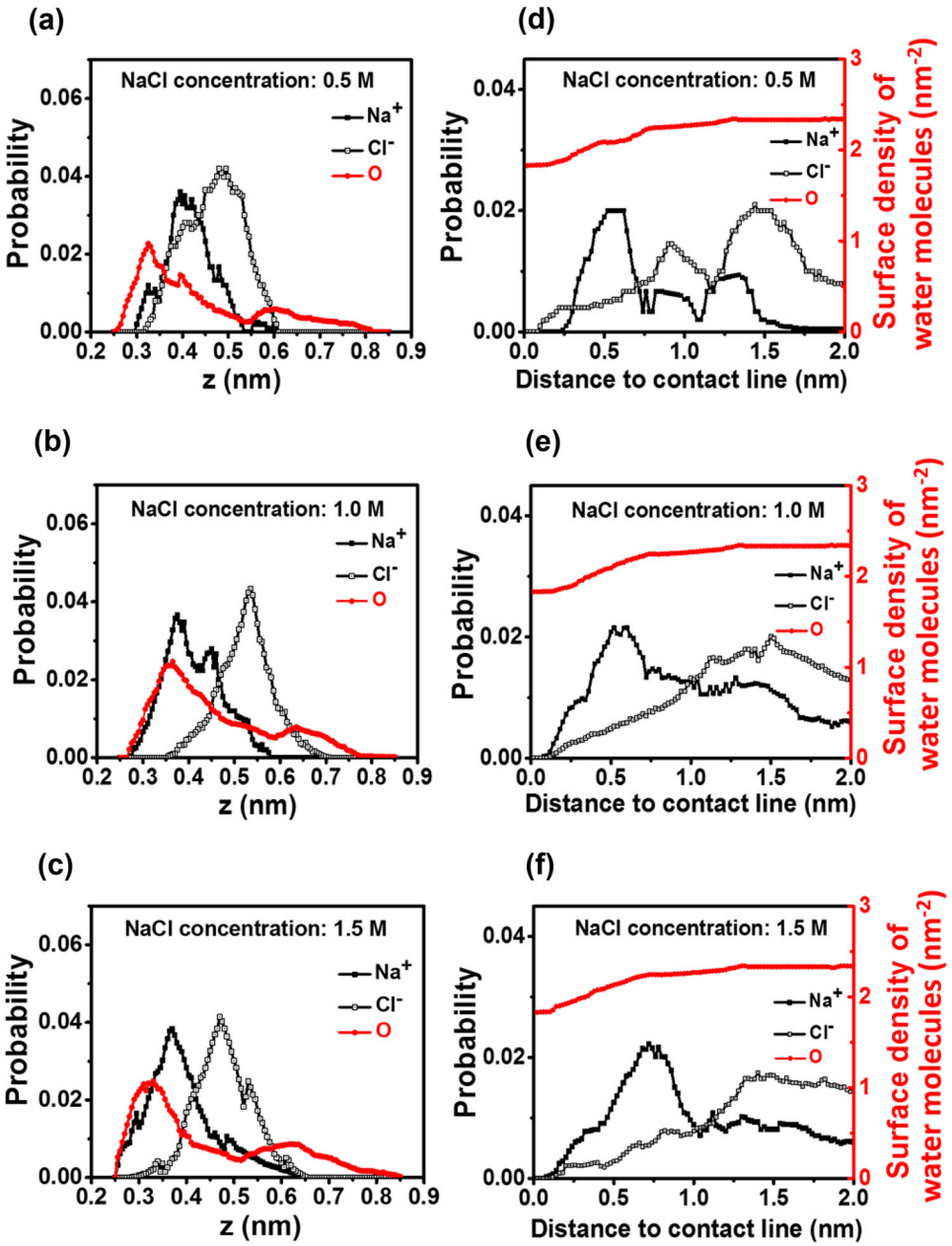

Fig. 5 Distribution of Na^+, Cl^-, and water molecules on patterned GO surfaces with different NaCl concentrations. **a–c** Distribution probability of Na^+, Cl^-, and water molecules along the z-direction for NaCl concentrations of 0.5 M (**a**), 1.0 M (**b**), and 1.5 M (**c**). **d–f** Distribution probability of Na^+/Cl^- ions and surface density of water molecules vs. distance to contact line for NaCl concentrations of 0.5 M (**d**), 1.0 M (**e**), and 1.5 M (**f**). The black solid squares, black hollow squares, and red circles represent Na^+, Cl^-, and water molecules, respectively. (Color figure online)

distribution of Na^+ ions is found to be closer to the contact lines.

As shown in Fig. 6a, as the NaCl concentration increases, the average number of H-bonds shows a slight decrease on patterned GO surfaces, which is consistent with the slight decrease in the water–water interaction energy. However, the average total interaction energy per outermost water molecule still increases, due to the increase in NaCl concentration (Fig. 2a). As shown in Fig. 6b, the $\tau_{\text{H-bond}}$ values show an obvious increase with the concentration of NaCl, which can be attributed to the clear increase in the average H-bond energy per outermost water molecule. (The average H-bond energies per outermost water molecule can be found in the ESI†.) The influence of Na^+ ions on the H-bonds lifetime of the outermost water molecules is more marked than that of Cl^- ions. The closer proximity of Na^+ ions to the contact lines improves the stability of the H-bonds involving the outermost water molecules, which hinders the diffusion of water across the contact lines, and reduces the number of water molecules evaporating from the unoxidized regions.

As the oxidized regions of patterned GO can have different oxidation degrees [51], we further investigated the evaporation of water with 1.0 M NaCl concentration on patterned GO surfaces with different oxidation degrees. Figure 7a shows that the evaporation rate does not change

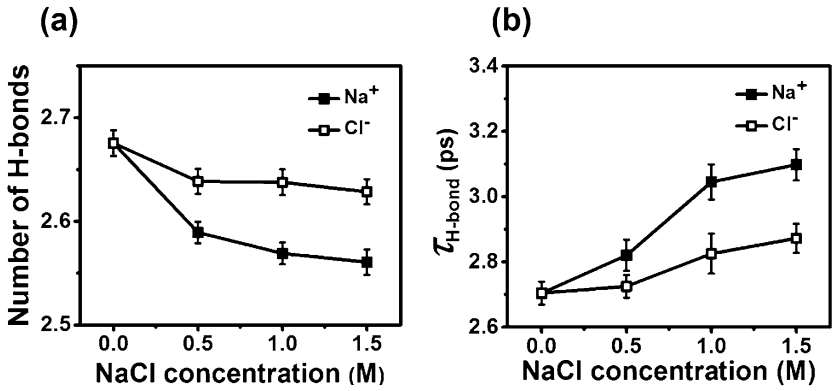

Fig. 6 Hydrogen bonding characteristics of outermost water molecules on patterned GO surfaces with different NaCl concentrations. **a** Average number of H-bonds for different NaCl concentrations. The black solid and black hollow squares represent the average number of H-bonds per outermost water molecule under the influence of Na^+ and Cl^- ions, respectively, on patterned GO surfaces with different NaCl concentrations. **b** Average lifetime of H-bonds for different NaCl concentrations. The black solid and black hollow squares represent the average lifetime of H-bonds per outermost water molecule under the influence of Na^+ and Cl^- ions, respectively, on patterned GO surfaces with different NaCl concentrations

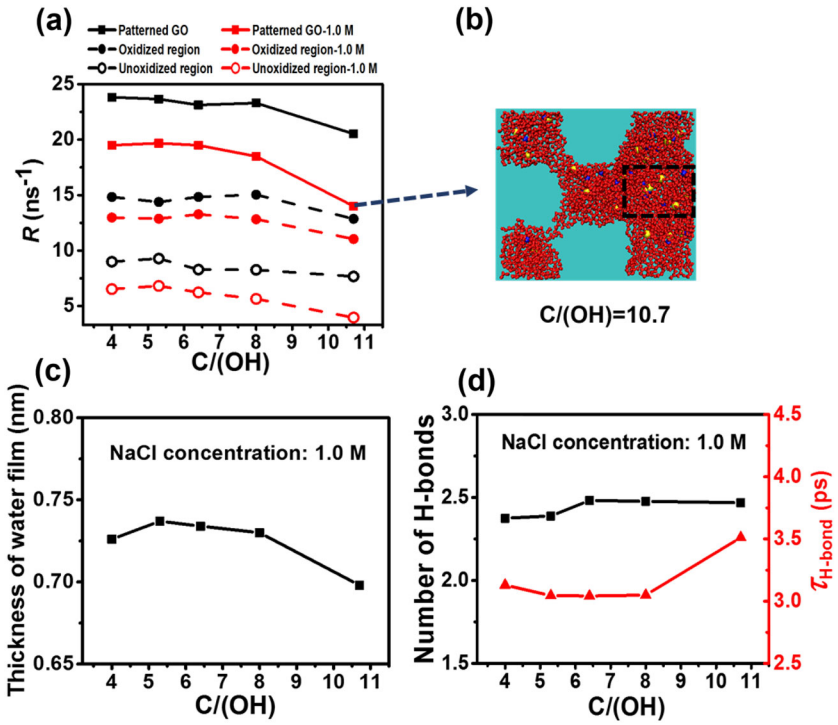

Fig. 7 (Color online) Evaporation of 2256 water molecules on patterned GO surfaces with 1.0 M NaCl concentration under different oxidation degrees. **a** Evaporation rate on patterned GO with and without 1.0 M NaCl. The black and red squares represent the total evaporation rate with and without 1.0 M NaCl, respectively. The black and red solid circles represent the evaporation rate on oxidized regions ($R_{oxidized}$) with and without 1.0 M NaCl, respectively. The black and red hollow circles represent the evaporation rate on unoxidized regions ($R_{unoxidized}$) with and without 1.0 M NaCl, respectively. **b** Snapshot of water and ions on patterned GO at C/(OH) = 10.7. The black dashed rectangle outlines a water film formed on the unoxidized region. **c** Water thickness on patterned GO with 1.0 M NaCl under different oxidation degrees. **d** Hydrogen bonding characteristics of outermost water molecules in the oxidized regions of patterned GO with 1.0 M NaCl, under different oxidation degrees. The black squares and the red triangles represent the average number and lifetime of H-bonds, respectively, per outermost water molecule

significantly when the C/(OH) ratio increases from 4 to 8. However, when C/(OH) reaches 10.7, the water evaporation rate shows a sharp drop. Figure 7b reveals that, as C/(OH) reaches 10.7, water and ions spread onto the unoxidized region, and Fig. 7c highlights a corresponding drop in the water thickness. Figure 7d shows that the number of

H-bonds per outermost water molecule remains almost constant when the oxidation degree changes. The $\tau_{H\text{-bond}}$ values show an obvious increase for C/(OH) = 10.7, which is mainly due to the reduction in water thickness. These results are highly consistent with our previous work with no ions included in the system [19], which shows that when the oxidation degree varies in a certain range, the effect of the Na^+ and Cl^- ions on the water evaporation is less significant.

4 Conclusion

In conclusion, we carried out MD simulations to investigate the influence of Na^+ and Cl^- ions on the evaporation of nanoscale water from graphene oxide surfaces. We found that the evaporation rate on both patterned and homogeneous GO surfaces decreases as the concentration of NaCl increases from 0 to 1.5 M, because the presence of the ions extends the H-bond lifetimes of the outermost water molecules. Compared with the homogeneous GO surfaces, the evaporation rate on patterned GO shows a higher decrease. Further analysis shows that the obvious decrease in evaporation rate on the unoxidized regions can be attributed to the increased amount of Na^+ ions near the contact lines. The proximity of Na^+ ions greatly extends the H-bonds lifetime of the outermost water molecules and reduces the number of water molecules diffusing from the oxidized to the unoxidized regions. Moreover, the effect of the Na^+ and Cl^- ions on the water evaporation is less significant when the oxidation degree varies in a certain range. Our findings indicate that the effect of the Na^+ and Cl^- ions on the evaporation of nanoscale water can be affected by the morphology of the solid surfaces; these results may find potential applications in achieving controllable evaporation of nanoscale liquids on a solid surface.

Acknowledgements We thank Haiping Fang, Yi Gao, Beien Zhu, Xiaoling Lei, Jige Chen, Shanshan Liang, Xing Liu, Jingyu Qi, Gang Fang, Zhi Zhu, Yizhou Yang, Chonghai Qi, Yangchao Lu, Yangjie Wang, Xiaomeng Yu, Zhongjie Zhu, Xiaoyan Li, Huishu Ma, Jie Jiang, and Liuhua Mu for their constructive suggestions and help.

References

1. G. Zarei, M. Homaee, A.M. Liaghat et al., A model for soil surface evaporation based on Campbell's retention curve. J. Hydrol. **380**, 356–361 (2010). https://doi.org/10.1016/j.jhydrol.2009.11.010
2. F.E. Rockwell, N.M. Holbrook, A.D. Stroock, The competition between liquid and vapor transport in transpiring leaves. Plant Physiol. **164**, 1741–1758 (2014). https://doi.org/10.1104/pp.114.236323
3. W. Tao, K.S. Lackner, A.B. Wright, Moisture-swing sorption for carbon dioxide capture from ambient air: a thermodynamic analysis. Phys. Chem. Chem. Phys. **15**, 504–514 (2012). https://doi.org/10.1039/c2cp43124f
4. A.S. Joshi, Y. Sun, Numerical simulation of colloidal drop deposition dynamics on patterned substrates for printable electronics fabrication. J. Disp. Technol. **6**, 579–585 (2010). https://doi.org/10.1109/jdt.2010.2040707
5. W.L. Cheng, W.W. Zhang, H. Chen et al., Spray cooling and flash evaporation cooling: the current development and application. Renew. Sust. Energ. Rev. **55**, 614–628 (2016). https://doi.org/10.1016/j.rser.2015.11.014
6. G. Duursma, K. Sefiane, A. Kennedy, Experimental studies of nanofluid droplets in spray cooling. Heat Transf. Eng. **30**, 1108–1120 (2009). https://doi.org/10.1080/01457630902922467
7. J.Y. Xiao, Z. Li, X.Z. Ye et al., Self-assembly of gold nanorods into vertically aligned, rectangular microplates with a supercrystalline structure. Nanoscale **6**, 996–1004 (2013). https://doi.org/10.1039/c3nr05343a
8. P. Liu, X. Huang, R. Zhou et al., Observation of a dewetting transition in the collapse of the melittin tetramer. Nature **437**, 159–162 (2005). https://doi.org/10.1038/nature03926
9. L.J. Zhang, J. Wang, Y. Luo et al., A novel water layer structure inside nanobubbles at room temperature. Nucl. Sci. Tech. **25**, 81–83 (2014). https://doi.org/10.13538/j.1001-8042/nst.25.060503
10. B. Sobac, D. Brutin, Thermal effects of the substrate on water droplet evaporation. Phys. Rev. E Stat. Nonlinear Soft. Matter Phys. **86**, 021602 (2012). https://doi.org/10.1103/physreve.86.021602
11. W. Mathers, Evaporation from the ocular surface. Exp. Eye Res. **78**, 389–394 (2004). https://doi.org/10.1016/s0014-4835(03)00199-4
12. N. Musolino, B.L. Trout, Insight into the molecular mechanism of water evaporation via the finite temperature string method. J. Chem. Phys. **138**, 134707 (2013). https://doi.org/10.1063/1.4798458
13. C. Maqua, G. Castanet, F. Lemoine, Bicomponent droplets evaporation: temperature measurements and modelling. Fuel **87**, 2932–2942 (2008). https://doi.org/10.1016/j.fuel.2008.04.021
14. J.P. Mcculley, J.D. Aronowicz, E. Uchiyama et al., Correlations in a change in aqueous tear evaporation with a change in relative humidity and the impact. Am. J. Ophthalmol. **141**, 758–760 (2006). https://doi.org/10.1016/j.ajo.2005.10.057
15. M.D. Webster, J.R. King, Temperature and humidity dynamics of cutaneous and respiratory evaporation in pigeons, *Columba livia*. J. Comp. Physiol. B. **157**, 253–260 (1987). https://doi.org/10.1007/bf00692370
16. H.S. Dong, S.H. Lee, J.Y. Jung et al., Evaporating characteristics of sessile droplet on hydrophobic and hydrophilic surfaces. Microelectron. Eng. **86**, 1350–1353 (2009). https://doi.org/10.1016/j.mee.2009.01.026
17. M. Lee, D. Lee, N. Jung et al., Evaporation of water droplets from hydrophobic and hydrophilic nanoporous microcantilevers. Appl. Phys. Lett. **98**, 5404 (2011). https://doi.org/10.1063/1.3541958
18. M. Elbaum, S.G. Lipson, How does a thin wetted film dry up? Phys. Rev. Lett. **72**, 3562 (1994). https://doi.org/10.1103/physrevlett.72.3562
19. R. Wan, G. Shi, Accelerated evaporation of water on graphene oxide. Phys. Chem. Chem. Phys. **19**, 8843–8847 (2017). https://doi.org/10.1039/c7cp00553a
20. M. He, D. Liao, H. Qiu, Multicomponent droplet evaporation on chemical micro-patterned surfaces. Sci. Rep. **7**, 41897 (2017). https://doi.org/10.1038/srep41897

21. Y. Guo, R. Wan, Evaporation of nanoscale water on a uniformly complete wetting surface at different temperatures. Phys. Chem. Chem. Phys. **20**, 12272–12277 (2018). https://doi.org/10.1039/c8cp00037a
22. G. Shi, L. Chen, Y. Yang et al., Two-dimensional Na–Cl crystals of unconventional stoichiometries on graphene surface from dilute solution at ambient conditions. Nat. Chem. **10**, 776 (2018). https://doi.org/10.1038/s41557-018-0061-4
23. X. Wang, G. Shi, S. Liang et al., Unexpectedly high salt accumulation inside carbon nanotubes soaked in very dilute salt solutions. Phys. Rev. Lett. **121**, 226102 (2018). https://doi.org/10.1103/physrevlett.121.226102
24. G. Shi, Y. Dang, T. Pan et al., Unexpectedly enhanced solubility of aromatic amino acids and peptides in an aqueous solution of divalent transition-metal cations. Phys. Rev. Lett. **117**, 238102 (2016). https://doi.org/10.1103/physrevlett.117.238102
25. G. Shi, Y. Ding, H. Fang, Unexpectedly strong anion-π interactions on the graphene flakes. J. Comput. Chem. **33**, 1328–1337 (2012). https://doi.org/10.1002/jcc.22964
26. J. Liu, G. Shi, G. Pan, Blockage of water flow in carbon nanotubes by ions due to interactions between cations and aromatic rings. Phys. Rev. Lett. **115**, 164502 (2015). https://doi.org/10.1103/physrevlett.115.164502
27. X. Nie, B. Zhou, C. Wang, Wetting behaviors of methanol, ethanol, and propanol on hydroxylated SiO_2 substrate. Nucl. Sci. Tech. **29**, 18 (2018). https://doi.org/10.1007/s41365-018-0364-6
28. A.S. Ansari, S.N. Pandis, Prediction of multicomponent inorganic atmospheric aerosol behavior. Atmos. Environ. **33**, 745–757 (1999). https://doi.org/10.1016/s1352-2310(98)00221-0
29. M. Colonna, V. Baran, S. Burrello et al., Exotic break-up modes in heavy ion reactions up to Fermi energies. Nucl. Sci. Tech. **26**, 124–130 (2015). https://doi.org/10.13538/j.1001-8042/nst.26.s20509
30. L. Francalanza, U. Abbondanno, F. Amorini et al., Competition between fusion-evaporation and multifragmentation in central collisions in $Ni^{58} + Ca^{48}$ at 25A MeV. Nucl. Sci. Tech. **24**, 82–88 (2013). https://doi.org/10.1088/1742-6596/420/1/012084
31. D. Li, G. Shi, F. Hong et al., Potentials of classical force fields for interactions between Na^+ and carbon nanotubes. Chin. Phys. B **27**, 098801 (2018). https://doi.org/10.1088/1674-1056/27/9/098801
32. G. Fang, J. Chen, Hindered gas transport through aqueous salt solution interface. J. Phys. Chem. C **122**, 20774–20780 (2018). https://doi.org/10.1021/acs.jpcc.8b05495
33. W.S. Drisdell, R.J. Saykally, R.C. Cohen, On the evaporation of ammonium sulfate solution. Proc. Natl. Acad. Sci. USA **106**, 18897–18901 (2009). https://doi.org/10.1073/pnas.0907988106
34. T. Furuta, A. Nakajima, M. Sakai et al., Evaporation and sliding of water droplets on fluoroalkylsilane coatings with nanoscale roughness. Langmuir **25**, 5417–5420 (2009). https://doi.org/10.1021/la8040665
35. K.C. Duffey, S. Orion, N.L. Wong et al., Evaporation kinetics of aqueous acetic acid droplets: effects of soluble organic aerosol components on the mechanism of water evaporation. Phys. Chem. Chem. Phys. **15**, 11634–11639 (2013). https://doi.org/10.1039/c3cp51148k
36. S. Sjogren, M. Gysel, E. Weingartner et al., Hygroscopic growth and water uptake kinetics of two-phase aerosol particles consisting of ammonium sulfate, adipic and humic acid mixtures. J. Aerosol Sci. **38**, 157–171 (2007). https://doi.org/10.1016/j.jaerosci.2006.11.005
37. P.Y. Chuang, R.J. Charlson, J.H. Seinfeld, Kinetic limitations on droplet formation in clouds. Nature **390**, 594–596 (1997). https://doi.org/10.1038/37576
38. W.S. Drisdell, R.J. Saykally, R.C. Cohen, Effect of surface active ions on the rate of water evaporation. J. Phys. Chem. C **114**, 11880–11885 (2010). https://doi.org/10.1021/jp101726x
39. A.M. Rizzuto, E.S. Cheng, K.J. Lam et al., Surprising effects of hydrochloric acid on the water evaporation coefficient observed by raman thermometry. J. Phys. Chem. C **121**, 4420–4425 (2017). https://doi.org/10.1021/acs.jpcc.6b12851
40. H. He, J. Klinowski, M. Forster et al., A new structural model for graphite oxide. Chem. Phys. Lett. **287**, 53–56 (1998). https://doi.org/10.1016/s0009-2614(98)00144-4
41. Y. Tu, M. Lv, P. Xiu et al., Destructive extraction of phospholipids from Escherichia coli membranes by graphene nanosheets. Nat. Nanotechnol. **8**, 594 (2013). https://doi.org/10.1038/nnano.2013.125
42. D. Chen, B. Feng, H. Li, Graphene oxide: preparation, functionalization, and electrochemical applications. Chem. Rev. **112**, 6027–6053 (2012). https://doi.org/10.1021/cr300115g
43. W.L. Jorgensen, J. Chandrasekhar, J.D. Madura et al., Comparison of simple potential functions for simulating liquid water. J. Chem. Phys. **79**, 926–935 (1983). https://doi.org/10.1063/1.445869
44. V.V. Zhakhovskii, S.I. Anisimov, Molecular-dynamics simulation of evaporation of a liquid. J. Exp. Theor. Phys. **84**, 734–745 (1997). https://doi.org/10.1134/1.558192
45. J.C. Phillips, R. Braun, W. Wang et al., Scalable molecular dynamics with NAMD. J. Comput. Chem. **26**, 1781–1802 (2005). https://doi.org/10.1002/jcc.20289
46. J.A.D. MacKerell, D. Bashford, M. Bellott et al., All-atom empirical potential for molecular modeling and dynamics studies of proteins. J. Phys. Chem. B **102**, 3586–3616 (1998). https://doi.org/10.1021/jp973084f
47. T. Darden, D. York, L. Pedersen, Particle mesh Ewald: an N·log(N) method for Ewald sums in large systems. J. Chem. Phys. **98**, 10089–10092 (1993). https://doi.org/10.1063/1.464397
48. R.B. Jackson, S.R. Carpenter, C.N. Dahm et al., Water in a changing world. Ecol. Appl. **11**, 1027–1045 (2001). https://doi.org/10.2307/3061010
49. Z. Zhu, H. Guo, X. Jiang et al., Reversible hydrophobicity-hydrophilicity transition modulated by surface curvature. J. Phys. Chem. Lett. **9**, 2346–2352 (2018). https://doi.org/10.1021/acs.jpclett.8b00749
50. R. Wan, C. Wang, X. Lei et al., Enhancement of water evaporation on solid surfaces with nanoscale hydrophobic-hydrophilic patterns. Phys. Rev. Lett. **115**, 195901 (2015). https://doi.org/10.1103/physrevlett.115.195901
51. L. Chen, G. Shi, J. Shen et al., Ion sieving in graphene oxide membranes via cationic control of interlayer spacing. Nature **550**, 380 (2017). https://doi.org/10.1038/nature24044